JOC *The Journal of Organic Chemistry*

Article

Beyond Size Complementary Factors in Anion−Tetralactam Macrocycle Complexes: From Intrinsic Gas-Phase to Solvent-Predicted Stabilities

Magdalena Zimnicka,* Kinga Kozłowska, and Witold Danikiewicz

Read Online

ACCESS | Metrics & More | Article Recommendations | Supporting Information

ABSTRACT: The gas-phase affinities of different types of anions X⁻ (halogen anions, oxoanions, and hydrogenated anions) toward a model tetralactam-based macrocycle receptor (**1**), defined in terms of stability of an anion−receptor complex (**1** + X⁻) against its disintegration, were evaluated by dissociation studies using a mass spectrometry-based methodology and supported by theoretical calculations (density functional theory−PBE0). The gas-phase complex with Cl⁻ was found to be tailor-made for the macrocycle **1**, while **1** + SA⁻ (SA⁻ = salicylate anion) and **1** + HSO₄⁻ were the weakest ones. Other complexes displayed a relatively low-stability dispersion (<1.2 kcal·mol⁻¹). The $1/\varepsilon_r$ approach of the electrostatic contribution scaling method was used to predict the stability trends in a dimethyl sulfoxide solvent from the gas-phase binding energy partition using the symmetry-adapted perturbation theory. High deformation energy and differences in solvation energies were suggested to be the main sources of inconsistency in the predicted and experimental stabilities of **1** + F⁻ and **1** + H₂PO₄⁻ complexes.
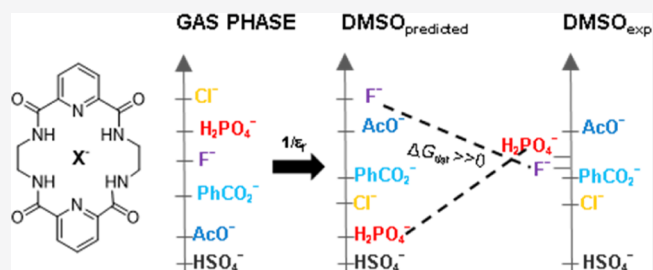
INTRODUCTION

Anions are ubiquitous in our artificial and natural environments. Their increasing omnipresence resulting from various industrial, agricultural, and daily life sources is both intended and harmful to the nature and living beings;[1] therefore, the manipulation of anion concentrations in order to regulate and remediate their unsustainable environmental and health exposure is widely applied by taking advantage from the anion recognition process.

Anion recognition is a process in which an anion selectively interacts with a receptor molecule according to the complementarity factors through noncovalent bonding. Thus, in the center of the anion−receptor interplays are various types of interactions including the most prevalent and, hence widely explored hydrogen bonding, electrostatic, σ-, π−hole-driven bonding, and these less common, utilizing solvophobic effects or coordinative bond formation with Lewis acidic metals.[2] The contribution of the particular interactions in the total energy of an anion−host complex determines its stability in different media. Hence, the widely exploited anion complexation utilizing hydrogen bonds is very sensitive to the polar and/or protic media because of the competitive solvation of anions that weakens the binding strength. The electrostatic forces, which dominate in the gas phase and nonpolar solvents ($\varepsilon_r < 4.7$; chloroform), are effectively reduced according to the inverse dielectric dependence for semipolar solvents ($4.7 < \varepsilon_r < 20.5$; acetone) to reach a neglected impact on anion−receptor stability.[3]

The structures of the receptor and anion and their mutual binding properties including proton affinity (PA), acid−base relationship, polarizability, and so forth determine the type of interactions that prevail in a given complex. Other factors that govern the selective propensity of an anion toward a receptor are related to the shape and size complementarity (geometrical factors). The electron-attractive potential of an anion has a higher power relationship than $1/r$ as experienced by a cation or neutrals. This results in its weakly bound and diffuse valence electron densities, offering a broad variety of accessible geometries.

The anion selectivity toward a given receptor requires many complementarity factors to be fulfilled. Beyond the specificity and selectivity of anion recognition in solutions, the intrinsic properties of an anion−receptor complex in the gas phase are of great importance because many computer-aided designs of new receptors and guided criteria are introduced in the solvent-free environment.[4] Earlier reported findings provided an approach to solution-phase anion affinities based on the gas-phase properties.[3] In this study, we evaluate the impact of anion properties on the gas-phase stability of an anion−

receptor complex. Although in many anion−receptor attractive systems, employing the hydrogen bonding interactions as widely explored in urea-based receptors, the anion selectivity follows the basicity trends,[5−8] any deviation from this trend may be ascribed to additional factors that are important for a given molecular system. Thus, the examination of the anion-type dependence on stability issue should provide the origin of the noncovalent attraction forces for a selected receptor system.

To address the abovementioned issues, the affinity of various anions toward one of the smallest and rigid tetralactam-based macrocycles **1** (Scheme 1) designed by Jurczak,[9] defined in

Scheme 1. Tetralactam-Based Macrocycle 1 and Selected Anions under Study

$X^- =$ F⁻
Cl⁻
Br⁻
NO_2^-
NO_3^-
AcO⁻
$PhCO_2^-$
Salicylate (SA⁻)
HSO_4^-
$H_2PO_4^-$
$H_2AsO_4^-$

1
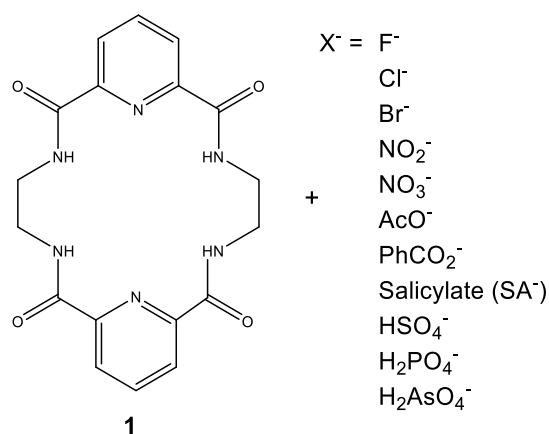
terms of the stability of an anion−receptor complex against its disintegration, was studied using a mass spectrometry (MS)-based methodology supported by theoretical calculations. The perturbation of the recognition process, while transferring the system into a polar milieu was further discussed in terms of the $1/\varepsilon_r$ approach[3] and compared with the available data for anion−receptor binding properties in the dimethyl sulfoxide (DMSO) solution. The reduced conformational freedom of both bare and anion-templated macrocycles allowed for a detailed structural analysis of their conformational space and

facilitated the multiple-factor and stability-governed analysis of recognition process. Although previous findings performed in DMSO solvent have found size complementarity as a dominant factor in the anion affinity properties of **1**, the analysis of the other stability components was not performed and is studied in detail in this study.

RESULTS AND DISCUSSION

In the presence of an anion X⁻ (Scheme 1), tetralactam **1** readily forms an associate, which is detected in the mass spectrum as a 1:1 complex, denoted as **1** + X⁻. The representative mass spectrum recorded for the solution of **1** containing F⁻ is shown in Figure 1. The other type of binding stoichiometry (2:1) constitutes a negligible contribution in the population of ions detected in the mass spectra, that is, 0.1−10% of the main 1:1 complex, depending on the anion type, analyte concentration, and electrospray ionization (ESI) ion source conditions. The presence of 2:1 aggregates in the case of oxoanions, as well as for some halides, implies the nonspecific aggregations rather than a specific characteristic solely for the carboxylate anion complexation through its syn−anti lone pairs, as suggested in previous studies.[9]

Intrinsic Gas-Phase Stability Studies Based on Collision-Induced Dissociation. The relative gas-phase stabilities of **1** + X⁻ complexes were evaluated by comparison of their dissociation energies using collision-induced dissociation (CID) experiments performed in a triple quadrupole mass spectrometer. In this approach, a complex ion is mass-selected by the first quadrupole (Q1) and undergoes collisions with N_2 collision gas in a collision cell. The internal energy of the ion increases as the CID energy (CE_{lab}) rises until it undergoes unimolecular dissociation according to Scheme 2.

Scheme 2. Dissociation Pathways Depending on the PA Balance between X⁻ and [1-H]⁻

$$\begin{array}{c} \text{[1-H]}^- + \text{HX} \quad PA(\text{[1-H]}^-) < PA(\text{X}^-) \\ \mathbf{1+X^-} \\ \text{X}^- + \mathbf{1} \quad PA(\text{[1-H]}^-) > PA(\text{X}^-) \end{array}$$
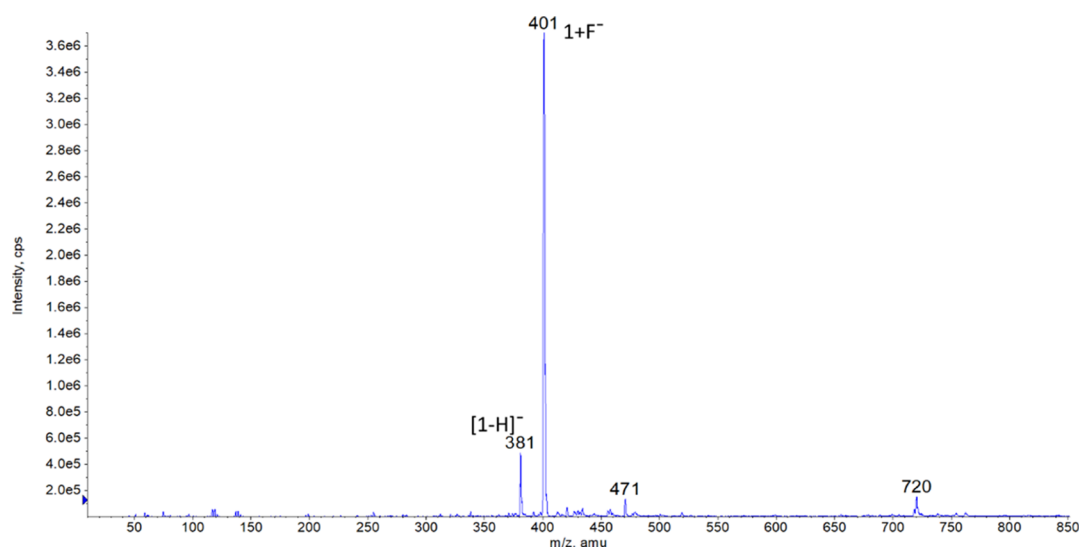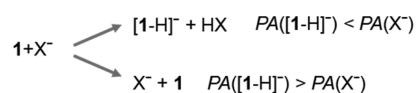
Figure 1. Q1 ESI-MS spectrum of a 1:1 mixture of **1** and (nBu)₄NF in methanolic solution.

Table 1. PA and GPB in kcal·mol⁻¹ of the Anionic Ligands and Deprotonated 1 vs the Observed Dissociation Products of 1 + X⁻ Complexes

anion (X⁻)	PA[a]	PA[b]	GPB[a]	GPB[b]	dissociation products
F⁻	370.7	372 ± 1	365.0	365.7 ± 0.2	1⁻
AcO⁻	347.1	343.2 ± 0.7 to 348.7 ± 2.2	340.7	341.5 ± 2.0	1⁻
PhCO$_2^-$	340.0	340.0 ± 2.9	332.3	333.0 ± 2.0	1⁻ and X⁻
NO$_2^-$	338.1	340.2 ± 0.2	330.7	333.7 ± 0.3	1⁻ and X⁻
1⁻	337.9				
Cl⁻	331.1	329.1 to 333.6 ± 2.1	325.7	328.3 ± 2.0	1⁻ and X⁻
H$_2$PO$_4^-$	327.6	330.5 ± 5.0	320.7	323.0 ± 4.9	X⁻
SA⁻	326.9	325.5 ± 2.2	319.5		X⁻
H$_2$AsO$_4^-$	325.9		319.7		X⁻
NO$_3^-$	322.1	324.5 ± 0.5 to 329.1 ± 5.8	314.7	317.8 ± 0.2	X⁻
Br⁻	321.7	320.6 to 323.4 ± 2.1	316.4	318.2 ± 2.0	X⁻
HSO$_4^-$	311.0	309.6 ± 5.4 to 316.8	303.4	302.3 ± 5.5	X⁻

[a]PA—proton affinity and GPB—gas-phase basicity calculated in this work (definitions of PA and GPB can be found in the Supporting Information). [b]Values from ref 10.

The observed ionic dissociation products depend on the PA balance between the anion X⁻ and the deprotonated macrocycle [1-H]⁻ (Scheme 2). Table 1 provides an overview on the proton affinities of anions X⁻, deprotonated 1, and the observed dissociation pathways. In the case of the most basic anions (PA(X⁻) > PA([1-H]⁻) = 337.9 kcal·mol⁻¹), proton transfer occurs producing a deprotonated macrocycle as the ionic dissociation product. The existence of the [1-H]⁻ + HX complexes, in which the intramolecular proton transfer from 1 to the more basic anion may take place, was excluded by calculations described later in this paper. For the X⁻ less basic than [1-H]⁻, the X⁻ dissociation product ion was observed. A small difference in the proton affinities between X⁻ and 1⁻ (ΔPA < 7 kcal·mol⁻¹) allowed the endothermic proton transfer to occur as the competitive dissociation pathway.

The raw dissociation energy of a given complex ion was determined from the analysis of its dissociation breakdown curve, representing the relationship between the applied, varied collision energy and the intensity of the peak corresponding to 1 + X⁻ (Figure 2). The x-intercept of the linear phase (a range of 20−80% of complex intensity) of the sigmoidal relationship between the applied collision energy and complex intensity was defined as the raw dissociation energy of complex (E_{1+X^-}).
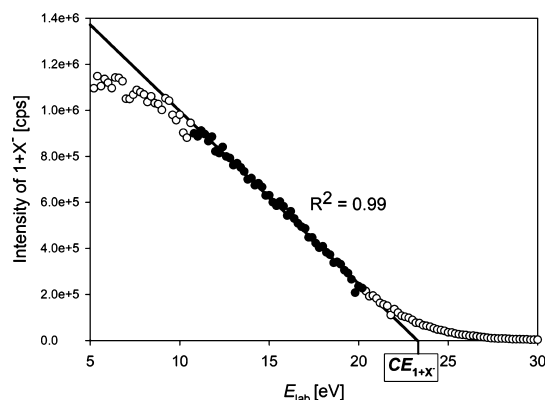
Figure 2. Energy-resolved dissociation breakdown curve of 1 + X⁻ (X = Cl). The linear section of the sigmoidal CID curve, which lays in the range of 20−80% of complex intensity, was used to determine the dissociation energy of 1 + X⁻ (E_{1+X^-}).

The varied abundance of the complex ion 1 + X⁻ under the increasing collision energy was used in constructing the CID breakdown curves instead of the total survival yield (ratio of the abundance of the precursor ion to the sum of abundances of the precursor and fragment ions). The dissociation of 1 + X⁻ complexes in a collision cell leads to fragment ions (Table 1) that have lower mass and energy compared to the precursor ions. Thus, the differences in the transmission of ions having dissimilar mass and energy may occur,[11] resulting in mass discrimination effects[12] and as a consequence of introducing substantial errors in the estimation of complex stability when the abundances of fragment ions were taken into account. To diminish the influence of the inaccurate abundance determination of fragment ions, solely the abundance of the complex ion 1 + X⁻ was monitored as a function of collision energy change (CE_{lab}).

All of the examined complexes showed similar dissociation curves to that shown in Figure 2. The raw dissociation energy values of 1 + X⁻, that is, the threshold CE in a laboratory frame (E_{1+X^-}), were determined according to the procedure described above directly from energy-resolved dissociation breakdown curves. This raw energy E_{1+X^-} corresponds to the kinetic energy gained by ions in the collision cell. As a result of collisions with neutral gas molecules in the collision cell, part of the kinetic energy of the ion is transferred into its internal energy. The maximum amount of kinetic energy available for absorption by the ion from this collision event in a single collision regime, according to conservation of energy and momentum in the collision, is called the center-of-mass energy (E_{cm}) and is given by eq 1

$$E_{cm} = E_{1+X^-} \frac{m_g}{m_g + m_i} \tag{1}$$

where E_{1+X^-} is the ion's laboratory kinetic energy and m_g and m_i are the masses of neutral gas and ion, respectively. In eq 1, the velocity of neutral is ignored because of its small thermal velocity compared to ion velocity. In general, this assumption is sufficiently accurate to estimate the upper limit of the energy transfer in a collision event. For processes taking place at a low laboratory frame kinetic energy of the ion (low-energy and/or high-mass ions), E_{cm} is determined by the temperature of collision gas.[13]

In general, the energy deposition and its distribution within the ion during the collisional activation are considered to affect

the dissociation process. Because the complex ions were formed under identical ESI ion source conditions and source parameters, the initial energy of the complexes should be the same and therefore its contribution to the internal energy of complex ions is skipped and only the portion of kinetic energy of the ion accelerated in the second quadrupole (Q2) is considered as an input of the ion internal energy.

E_{cm} is only a basic approximation of the energy available in the ion and does not take into account the real efficiency of energy transfer into the internal modes in a collision event. In a more accurate approximation, the relationship between the number of collisions and collision cross section (CCS) was considered. In this simple approach, the stepwise kinetic energy loss during sequences of collision processes also related to the CSS of an ion was omitted. The increase of the CCS of the ion complex results in more energy deposition within an ion by increasing the number of collisions with a neutral target. Therefore, in the more accurate approximation, the CCS values of complex ions were considered using the reduced eq 2[14] for the internal energy acquired by ions passing through a collision cell

$$E_{int} = E_{cm} \cdot n l \sigma \qquad (2)$$

The energy transfer in the collision events described by eq 2 is thus additionally influenced by the collision gas pressure (n—gas number density), CCS of ions (σ), and the length of the collisional trajectory (l—length of the collision cell). Equation 2 is valid on the assumption of the total transfer of the center of mass kinetic energy to the initial energy in a single collision. The center-of-mass energy conversion into ion internal energy was suggested to be highly efficient for large molecules ($\approx100\%$),[15] whereas for smaller systems, the lower energy deposition is expected.[16] However, taking into account the structural similarity of the analyzed complexes, the errors associated with this kinetic to internal energy transfer should lead to a systematical bias of the dissociation energy; hence, the minor influence on the affinity trends studied in this work is expected. The identical collision conditions, that is, the same pressure and collision cell length, allowed for the center-of-mass dissociation energies to be only multiplied by the CCSs of ion complexes to obtain the CCS correction of relative dissociation energies (E_{int}). The CCSs of complexes under study were obtained by cavity surface area approximation.[17] In this approach, the σ value is directly calculated from the solvent cavity surface area parameter generated by the conductor polarizable continuum model (for detailed values, please see Table S1 in the Supporting Information). The results of these two approaches to the dissociation energies (Table 2) of the complexes were further compared with the theoretical values.

Structures of 1 + X⁻ Complexes—A Theoretical Approach. The model macrocycle 1 has two aromatic pyridine subunits intertwined symmetrically into the tetralactam cyclic structure. It poses four amide hydrogen atoms directed into its cavity readily to stabilize an anionic ligand (X^-) in its interior cavity via formation of the $N-H{\cdots}X^-$ system of hydrogen bonds. The presence of a basic pyridine moiety may additionally enhance the stability with hydrogenated anions by acting as a hydrogen bond acceptor.

In contrast to one stable conformation revealed by the X-ray crystallographic study,[9] two distinguished conformers differing in the symmetry of free macrocycle 1 were found from a theoretical conformational search (Figure 3). The plane

Table 2. Experimental Dissociation Energies of 1 + X⁻ Given as a Center-of-Mass Energy (E_{cm}) and Corrected by Collision Cross Section (E_{int})

complex (1 + X⁻)	m/z	E_{1+X^-} [eV]	E_{cm} [eV]	E_{int} [eV·Å²]
1 + F⁻	401	16.1	1.05	189.8
1 + AcO⁻	441	16.1	0.96	182.0
1 + PhCO₂⁻	503	19.2	1.01	207.1
1 + NO₂⁻	428	17.8	1.10	204.4
1 + Cl⁻	417	23.2	1.46	267.3
1 + H₂PO₄⁻	479	19.4	1.07	204.6
1 + SA⁻	519	15.3	0.78	161.8
1 + H₂AsO₄⁻	523	18.6	0.95	182.9
1 + NO₃⁻	444	17.0	1.01	189.2
1 + Br⁻	461	18.7	1.07	197.3
1 + HSO₄⁻	479	15.5	0.85	161.1

symmetrical structure with the two parallel C−C linkers of amide groups in the tetralactam structure and an antiparallel pyridine subunit arrangement (as is well seen in a side view projection in Figure 3) is 1.4 kcal·mol⁻¹ more stable than the C_2-symmetric structure with perpendicular C−C bond positions. The amide NH positions, relevant for the formation of stabilizing intramolecular hydrogen bonds between pyridine-N and amide-H as observed in similar systems, in pyridine-2-carboxamide or pyridine-2,6-dicarboxamide derivatives,[18−20] are supposed to be responsible for this difference in conformer stability.

In 1-parallel, two adjacent to each pyridine unit amide NH groups remain in its plane, giving rise to the formation of two hydrogen bonds between pyridine-N and amide-H (N···H 2.260 Å). In contrast to 1-parallel, in the higher energy conformer, the NH groups adopt a scissor-like conformation, up and down from the near flat plane of the pyridine moieties. Thus, the planarity effects must play a stabilizing role here. The mutual arrangement of pyridine moiety and amide groups results in position of amide hydrogen atoms in-plane arrangement for 1-parallel conformation or constrains the significant distortion of this plane (1-perpendicular, H11−H14−H5−H9 dihedral = 44°). The 1-parallel conformer is analogous to the reported crystal structure of 1 (Figure S1a, Supporting Information).[9]

The complexation with an anion evokes the conformational changes in 1 to ensure the effective solvation of the anion. Such conformational reorganization mainly involves the changes of dihedral angles of the aliphatic part of 1 to allow for redirection of amide hydrogen atoms directly toward the anionic center. As a consequence, the dihedral angle between the two planes of aromatic moieties, for both parallel and perpendicular conformers, is lower than that for a near-flat unbound macrocycle (the representative structures of 1 + Cl⁻ are shown in Figure 4a). Moreover, in the case of 1-perpendicular conformer, upon the complexation, the out-of-plane distortion of amide hydrogens decreases to H11−H14−H5−H9 dihedral 10−20°, depending on the complex structure.

The macrocycle 1 seems to be a one-site-binding system, that is, four amide hydrogen atoms interact with one anion center by forming four strong, quadfurcated, and nearly symmetrically equivalent hydrogen bonds (Figure 4a). Even for carboxylate ions (acetate, benzoate, and salicylate) for which the two-center binding mode might be expected with both carboxylate oxygen atoms involved in the formation of
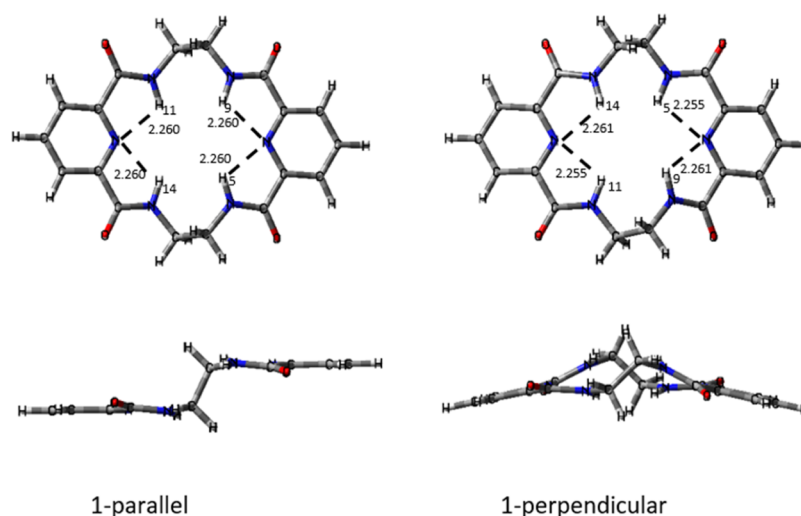
Figure 3. Two projections of two conformations of **1**: upper projection—a view on a mean plane of macrocyclic ring and lower projection—representing a lateral view.
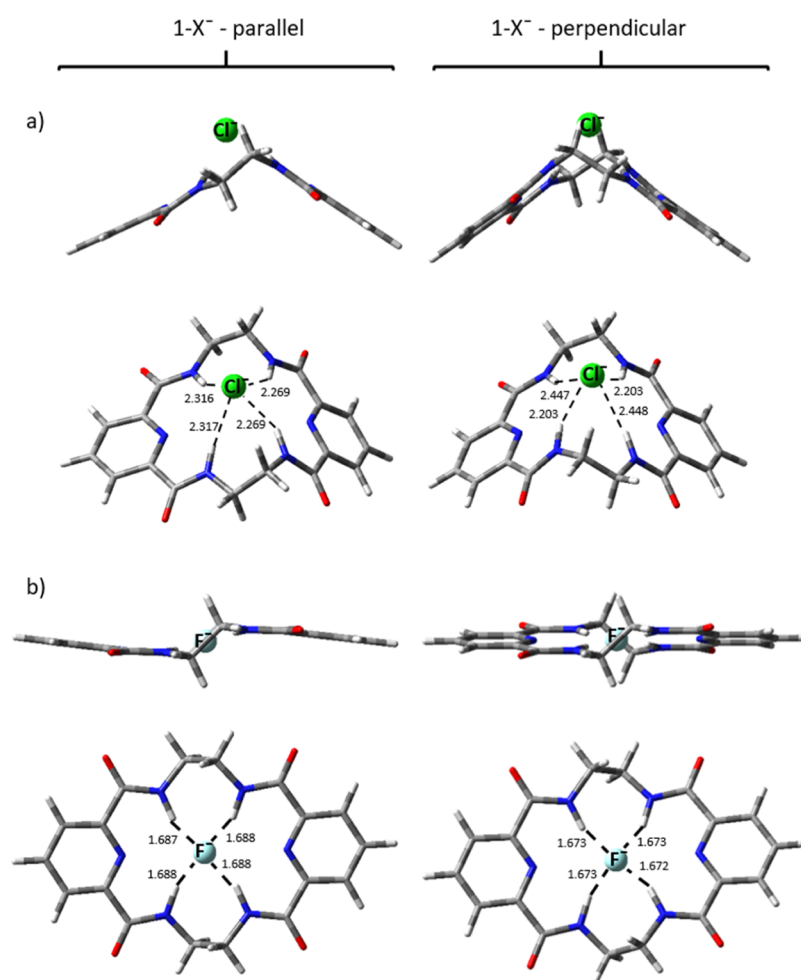
Figure 4. Theoretical structures of two conformers of (a) **1** + Cl⁻ and (b) **1** + F⁻ complexes shown in two projection modes: upper—a lateral view and lower—a more planar view showing the main binding site formed by the hydrogen bonds between the amide-H atoms and X⁻. The intramolecular hydrogen bonds between N−H and pyridine-N within **1** are omitted for clarity.

the hydrogen bonding system, similar to that observed for urea-based receptors,[21] or anions rich in oxygen atoms enabling to a higher binding states, the one-center arrangement is postulated by theoretical studies. The hydrogen bond

between the available hydrogen atoms of the OH group of anions and macrocyclic-N as an acceptor additionally stabilizes the complexes with hydrogen sulfate, dihydrogen phosphate, and dihydrogen arsenate anions (Figure S2). Additionally, the

Table 3. Relative Energies of $1 + X^-$ (ΔE_0, ΔH_{298K}, and ΔG_{298K}), That Is, the Energy Differences between the Most Stable and Less Stable Conformations in kcal·mol^{-1} and Their Calculated Chemical Hardness (η)

complex ($1 + X^-$)	$1 + X^-$-parallel				$1 + X^-$-perpendicular			
	ΔE_0	ΔH_{298}	ΔG_{298}	η [eV]	ΔE_0	ΔH_{298}	ΔG_{298}	η [eV]
$1 + F^-$	0.6	0.6	0.7	2.66	0	0	0	2.67
$1 + AcO^-$	0	0	0	2.33	0.7	0.8	0.6	2.30
$1 + PhCO_2^-$	0	0	0.2	2.41	0	0	0	2.43
$1 + NO_2^-$	0.3	0.3	0.3	2.00	0	0	0	2.02
$1 + Cl^-$	0	0	0	2.45	0	0	0	2.47
$1 + H_2PO_4^-$	0	0	0	2.60	0.3	0.4	0.1	2.58
$1 + SA^-$	0.4	0.4	0.5	2.20	0	0	0	2.23
$1 + H_2AsO_4^-$	0	0	0	2.62	0.5	0.4	0.7	2.61
$1 + NO_3^-$	0.1	0.1	0.2	2.46	0	0	0	2.48
$1 + Br^-$	0	0	0	2.23	0	0	0	2.24
$1 + HSO_4^-$	0	0	0	2.56	0.9	0.9	1.0	2.54

weak interactions between the C−H donors of the C−C linkers of amide groups in tetralactam with anions possessing the second acceptor of the hydrogen bond may additionally complement the intermolecular interactions.

The anion center is asymmetrically positioned above the mean plane of the macrocycle in $1 + X^-$-parallel, while in $1 + X^-$-perpendicular, it remains outside the macrocyclic cavity, arranging on or near the macrocyclic axis of symmetry (Figures 4a and S2). Only for F$^-$ (Figure 4b), this tetragonal pyramidal arrangement around the anionic center is dropped in favor of placing F$^-$ directly in the central position of the macrocyclic cavity on the near right (the H11−H14−H5−H9 dihedral is 0.14°) or distorted (the H11−H14−H5−H9 dihedral 20.5°) plane formed by amide hydrogen atoms, for parallel and perpendicular conformations, respectively.

The theoretically derived structures of 1, $1 + Cl^-$, $1 + AcO^-$, and $1 + F^-$ represented by parallel conformation are very similar to those obtained earlier from crystallographic data (the superimposed theoretical and crystal structures[9] are shown in Figure S1b,c). The Gibbs free energy difference between the parallel and perpendicular conformers of $1 + X^-$ (Table 3) is very small. The parallel conformation, as the solely populated in the crystal phase, for majority of the studied complexes is less stable than that represented by the perpendicular conformation. The parallel conformer is more stable only for anions possessing the additional hydrogen bond donor group able to coordinate to the nitrogen atom of pyridine moiety, as for hydrogen sulfate, dihydrogen phosphate, dihydrogen arsenate anions, and acetate anions.

Although the macrocycle 1 and its noncovalent complexes seem to belong to a relatively rigid system as represented by a single parallel conformation in the crystal state, the theoretical structural considerations led to the two distinguished conformations of the tetralactam scaffold with parallel and perpendicular positioned C−C bonds. The flexibility of this molecular system is apparently lower for a bare macrocycle (the energy barrier between conformers is calculated to be 8.8 kcal·mol^{-1}) than for an anion-bound structure by 4.2 kcal·mol^{-1} as calculated for $1 + Cl^-$.

The origin of the stability difference between the two types of conformers was examined using one of the theoretical chemical reactivity descriptors, the chemical hardness (η).[22,23] This parameter refers to the resistance of a given molecular system to change in its electron density distribution and is defined by density functional theory (DFT) as the second derivative of electronic energy with respect to the number of

electrons for a constant external potential. By applying the finite difference approximation and Koopman's theorem, the chemical hardness is directly calculated from frontier molecular orbital energies as half the energy gap between the lowest unoccupied molecular orbital and the highest occupied molecular orbital according to eq 3

$$\eta = \frac{1}{2}(E_{\text{LUMO}} - E_{\text{HOMO}}) \tag{3}$$

The chemical hardness of $1 + X^-$ complexes (Table 3) well agrees with the relative stability between the two available conformations, that is, a more stable conformer has a larger value of η. It is worth to underline here that the stability described by the hardness descriptor relates to the reactivity of a molecular system toward the perturbation in electron distribution at its ground state; hence, this approach is relevant for the chemical system in which the electronic distribution is important with respect to the other stability factor—molecular orbital interactions.

Theoretical versus Experimental Stability of $1 + X^-$. The theoretical stabilities of $1 + X^-$ complexes (Table 4) were calculated for the reaction scheme, according to the dissociation pathway observed in the gas-phase collision experiments, based on Scheme 2. The relationship between experimentally derived stabilities (E_{cm}) and computed values is presented in Figure 5. The theoretical stabilities were also fitted to the experimental E_{int}; however, a poorer relationship was obtained ($R^2 = 0.7$). This may be due to the fact that both E_{cm} and σ values have no proportional contribution in the ion's internal energy (the σ values are 2 orders of magnitude higher than the E_{cm} values), and hence, the resulting E_{int} is very sensitive to insufficiently accurate calculations of the CCS. Taking into account the relevant σ factor in eq 2, the use of E_{int} may not lead to the expected improvement in the description of the available internal energy of similarly shaped ions.

The data derived from both calculations and experiments clearly show that the most stable complex is $1 + Cl^-$, while $1 + SA^-$ and $1 + HSO_4^-$ are the weakest ones. Other complexes display relatively low-stability dispersion (<1.2 kcal·mol^{-1}). To evaluate the influence of the calculation method on the theoretical stability values of $1 + X^-$, the calculations with the additional two methods, ωB97XD (the latest range separated functional from Chai and Head-Gordon, enabled capturing both short- and long-range interactions with empirical dispersion included)[28] and Truhlar's M06-2X global hybrid functional,[29] were compared in terms of the variation of both

Table 4. Adiabatic Dissociation Energies (ΔE_0 with ZPVE Included, ΔH_{298}, and ΔG_{298})[a] in kcal·mol^{-1} of 1 + X$^-$ Computed According to the Experimentally Derived Dissociation Scheme and the Earlier Reported Association Constants (K_{ass}) Determined by ^{1}H NMR Titration[9,24] Along with the pK_a of HX

complex (1 + X$^-$)	ΔE_0	ΔH_{298}	ΔG_{298}	K_{ass} [M^{-1}] in DMSO	pK_a of HX in H$_2$O (in DMSO)
1 + F$^-$	42	43	34	830 ± 120	3.17 (15)[25]
1 + AcO$^-$	45	45	31	2640 ± 270	4.75 (12.6)[26]
1 + PhCO$_2^{-b}$	44	43	31	202 ± 20	4.20
1 + NO$_2^{-b}$	46	46	35		
1 + Cl^{-b}	48	48	39	65 ± 10	−6.10 (1.8)[27]
1 + H$_2$PO$_4^-$	47	47	33	1680 ± 110	2.16
1 + SA$^-$	40	40	26		
1 + H$_2$AsO$_4^-$	45	45	31		
1 + NO$_3^-$	43	43	30		
1 + Br$^-$	43	43	34		
1 + HSO$_4^-$	40	41	26	<5	−3.00

[a]Calculated for the adiabatic process but maintaining the conformation type (parallel or perpendicular) of the macrocycle. The ΔG_{298} calculated for the adiabatic process for dissociation leading to the most stable macrocyclic conformer exhibits poorer correlation with the experimental data (Figure S3). [b]The given values are for the lowest dissociation energy pathway (Scheme 2).
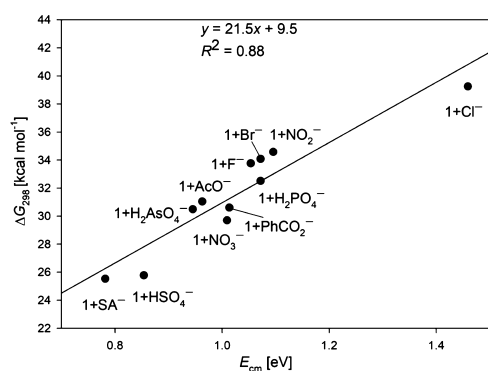
Figure 5. Relationship between the experimentally derived stabilities given as E_{cm} and the theoretical stabilities calculated as ΔG_{298} for the dissociation of 1 + X$^-$ (Table 4).

geometry and energy aspects. Although the optimization geometry using the tested methods led to essentially very similar structures (the root-mean-square deviation of atomic positions obtained after superposing the structures of 1 + Cl$^-$ complex derived from three computational methods (Figure S4) was less than 0.0384 Å with a root-mean-square maximum difference of 0.0517 Å), the dissociation energies calculated with PBE0, ωB97XD, and M06-2X functionals with the same basis set (6-311++G**) displayed larger spread (Figure 6). This discrepancy was more pronounced for the complexes with halogen anions, especially in the case of fluorides ($\Delta\Delta G$ = 4.4 kcal·mol^{-1}) than for oxoanions ($\Delta\Delta G$ < 2 kcal·mol^{-1}). The increase of the computation accuracy by a single point energy recalculation with a higher basis set at M062X/aug-cc-pVTZ changed the ΔG by less than 0.5 kcal·mol^{-1} and showed a little improvement in consistency between the experimental and theoretical stabilities (R^2 = 0.89).

The results described above underlined the importance of the computational effort put into obtaining reliable results; nevertheless, this higher precision is required for systems having very similar stabilities. In our case, the stability shifts were observed in a narrow region on the stability relationship curve while keeping clear evidence of the most and least stable gas-phase associates.

Similar to the results obtained in the DMSO solution (Table 4),[9,24] the stability series of 1 + X$^-$ do not match the basicity of anions (Figure S5), although in a similar macrocyclic system, this type of correlation was observed.[8] The previous studies underlined the importance of the macro ring size complementarity in anion recognition in such a design receptor 1 family.[24] The comparison of the most stable complex in the gas phase, which is 1 + Cl$^-$, and in DMSO-1 + AcO$^-$ puts forward the consideration of another relevant aspect, associated with the solvent effects. If the anion's size matching plays a major role in anion recognition by 1, similar stability trends would be expected in the gas phase. This feature, that is, the influence of the solvent on the stability of this family of macrocyclic anionic acceptors, was not considered earlier; however, as it is evident from our studies, it may play a crucial role in determining the efficiency and specificity of the anion recognition process.

The origin of the gas-phase stability of the examined complexes has been further explored by the analysis of physically meaningful components of interaction energy
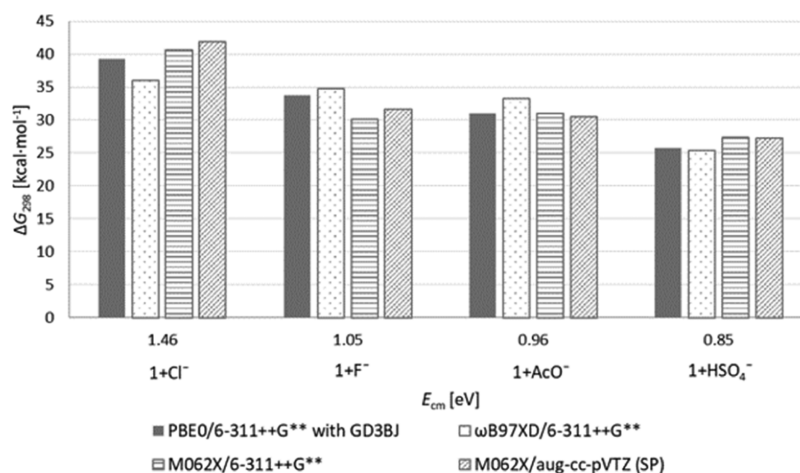
Figure 6. Theoretical dissociation energy (ΔG_{298}) of selected 1 + X$^-$ complexes obtained by different DFT methods.

Table 5. Components of the SAPT0 Interaction Energy [kcal·mol^{-1}] for the Considered Complexes

$1 + X^-$	electrostatics	induction	dispersion	exchange	total
1 + F$^-$	−77.6	−48.0	−2.3	31.4	−96.4
1 + AcO$^-$	−49.8	−29.6	−12.7	22.4	−69.7
1 + PhCO$_2^-$	−44.8	−24.8	−14.7	19.1	−65.3
1 + NO$_2^-$	−48.6	−29.7	−8.8	22.3	−64.8
1 + Cl$^-$	−45.5	−36.6	−9.8	31.3	−60.6
1 + H$_2$PO$_4^-$	−48.5	−24.9	−12.8	21.4	−64.7
1 + SA$^-$	−40.5	−22.5	−14.5	17.6	−59.9
1 + H$_2$AsO$_4^-$	−48.1	−26.0	−13.5	23.6	−64.0
1 + NO$_3^-$	−41.6	−21.0	−9.6	15.3	−57.0
1 + Br$^-$	−40.1	−37.0	−10.3	34.4	−53.0
1 + HSO$_4^-$	−42.7	−20.8	−12.9	19.2	−57.3

between the macrocycle and the anion, that is, electrostatic, induction, dispersion, and exchange terms using the symmetry-adapted perturbation theory—SAPT.[30] The simplest truncation of SAPT, denoted as SAPT0, was used to compute the total interaction energy and to group individual terms into relevant energy components (Table 5).

The main source of the interactions within **1** + X$^-$ is as expected electrostatic forces because of the electrostatic character of a main hydrogen bonding interaction. The induction constitutes the second binding component, about half of the electrostatic stabilization. The correlation between the SAPT total interaction energy and the DFT-calculated interaction energies for vertical process ($-E_v^0$, the sign change of the DFT-computed energy is required because the DFT-derived energies correspond to the dissociation reaction—Scheme 2), that is, without taking into account the relaxation of the anion and a macrocycle molecule following complex disintegration, which more reflects the SAPT-computed energies, may be seen as a simple check of the utilization of the SAPT approach to the description of anion−macrocycle interactions in a gas phase (Figure S6). The subtle differences of anion affinities toward **1** obtained by SAPT description are consistent with the DFT-derived results. The total binding energies correlate well ($R^2 = 0.98$) with the DFT $-E_v^0$ counterpoise-corrected energies.

$1/\varepsilon_r$ Approach to Stability Trends in DMSO from the Gas-Phase Properties. Taking advantage of the generated SAPT energy components, we predicted the stability trends of the selected complexes in DMSO (ΔG_{DMSO}^{pred}) according to the earlier reported $1/\varepsilon_r$ approach[3] and compared these predicted values with the experimentally derived stabilities of **1** + X$^-$ reported in DMSO.[9] For this purpose, eq 4 was considered to obtain stability trends in DMSO from $1/\varepsilon_r$-scaled electrostatic contribution to the gas-phase dissociation energy (ΔG_{298v}).

$$\Delta G_{DMSO}^{pred} = \Delta G_{298v} + \left(\frac{1}{\varepsilon_r} - 1\right) \times \frac{E_{elst}(SAPT)}{E_{Tot}(SAPT)}\Delta G_{298v}$$

$$(4)$$

The predicted stability values (Figure 7) correlate with the experimental DMSO binding strength with two exceptions of **1** + F$^-$ and **1** + H$_2$PO$_4^-$. The source of this inconsistency between experimental and predicted stability orders may be related to the deformation factors associated with both macrocycle **1** and anions upon complexation/dissociation, not included in eq 4.

The $1/\varepsilon_r$ approach to the solution binding affinities from the computed gas-phase properties was originally developed for triazolophane, which belongs to the exceptional case of shape-
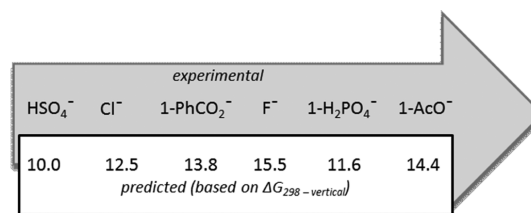
Figure 7. Comparison of experimental (DMSO) and predicted stability trends.

persistent receptors upon complexation reaction. Therefore, the deformation energy was negligible and hence was omitted in eq 4. In our case, although the conformational diversity of macrocycle **1** and its complexes is limited and the macrocyclic receptor within **1** + X$^-$ has very similar conformations for all of the examined anions (Figure S2 in the Supporting Information), except for the complex with F$^-$, the deformation factors associated with both macrocycle **1** and anions may have a significant influence on the prediction of stability trends based on eq 4. The deformation effects may be quantitatively described as the energy difference between adiabatic and vertical dissociation (ΔG_{def}(total), Table 6).

Table 6. Deformation Energies, ΔG_{def}(Total) Computed as a Difference between the Vertical and Adiabatic Dissociation Energy of 1 + X$^-$ Complexes, the Contribution of the Receptor Deformation (ΔG_{def}(1) in Total Deformation, and the Overall Impact on Deformation Energy in Complex Energy in kcal·mol^{-1}

$1 + X^-$	ΔG_{def}(total)	ΔG_{def}(**1**)/ΔG_{def}(total)	ΔG_{def}(total)/ΔG_{298}
1 + F$^-$	39	NA	1.2
1 + AcO$^-$	17	NA	0.5
1 + PhCO$_2^-$	11	NA	0.4
1 + Cl$^-$	6	1.0	0.1
1 + H$_2$PO$_4^-$	11	0.6	0.3
1 + HSO$_4^-$	11	0.5	0.4

The very high ΔG_{def}(total) in the case of **1** + F$^-$ complex indicates the high endothermic receptor conformation rearrangement upon the dissociation event preceded by proton transfer, which effectively diminishes the favorable affinity of F$^-$ toward **1**. For the remaining complexes, ΔG_{def}(total) constitutes variable contribution in ΔG_{298}. Interestingly, the lowest ΔG_{def}(total) was obtained for **1** + Cl$^-$, the most stable complex in the gas phase. This suggests that the deformation factors have a relevant influence on the intrinsic stability of **1**-

X^- complexes. As expected for the more complex anion structures, the additional anion deformation becomes significant, as $(\Delta G_{def}(1)/\Delta G_{def}(total))$ drops down for hydrogenated anion complexes. Another important factor that may account for the inaccuracy of the $1/\varepsilon_r$ approach is different solvation energies of anions. This factor may be dominant in the case of structurally different anions as for $H_2PO_4^-$.

In general, the stability trends derived from the $1/\varepsilon_r$ approximation are consistent with the experimental stability order despite the fact that $\Delta G_{def} \neq 0$. This suggests that the affinities of anions toward **1** may be described by $1/\varepsilon_r$, provided that the deformation energies of the complexes are similar and under consideration of the structurally similar anions.

CONCLUSIONS

The intrinsic gas-phase affinities of selected anions toward the model tetralactam-based macrocycle receptor (**1**), studied in this work both experimentally and theoretically, significantly differ from the values earlier reported for the DMSO solvent. The concept of size complementarity of anions to macrorings as a main force driving the binding properties, earlier postulated for this family of receptors seems to be incomplete in the light of our research. The studies in the gas phase revealed that the deformation factors upon dissociation govern the stability issues in this relatively rigid family of receptors; therefore, the medium reactive anion Cl^- has the highest affinity toward **1**.

Our studies gave the first evidence of the usefulness of the recently proposed $1/\varepsilon_r$ approach of the electrostatic term scaling method to predict the stability trends in the DMSO solvent from the gas-phase binding energy. Although in the analyzed systems $\Delta G_{def} \neq 0$, this method correctly predicted the stability trends in DMSO of complexes having similar deformation energy. Any significant increase of deformation energy leads to the overestimated values of stabilization energy. The other factor that may lead to inconsistency in predicting the stability properties is the significant difference in the solvation energy of anions, resulting from their structures.

Finally, the overall conclusion from our studies concerns the significant role of deformation energy in tuning the affinity of anions toward a given receptor, which should be considered while designing a new macrocyclic receptor. Further ongoing experimental and computational studies are aimed at considering the impact of deformation energy term on the $1/\varepsilon_r$-predicted solution-phase binding properties across various solvents, as well as including the solvation energy of anions, in predicting the binding trends based on the gas-phase properties.

EXPERIMENTAL SECTION

Materials. Macrocycle **1** was synthesized according to a literature procedure.[9] nBu$_4$NX salts were purchased from Sigma-Aldrich.

MS Measurements. Gas-phase stability data were obtained from the collision experiments (CID analysis) using the API 3000 mass spectrometer. The methanol solution containing the macrocycle **1** (c = 0.02 mM) and a given anion in the form of a tetrabutylammonium salt in a 1:1 ratio was infused to the electrospray ion source at a flow rate of 20 μL/min. The samples were analyzed in a negative ion mode with a capillary voltage at −4.5 kV, a declustering potential of 20 V, and an entrance potential of 10 V. The energy-resolved dissociation breakdown curves were recorded in CID and multiple reaction monitoring scanning modes. Nitrogen was used as a collision gas. In both scanning methods, the intensity of a peak corresponding to the given complex anion was monitored as a function of the increasing CE. Both of the scanning methods led essentially to the same results.

Computations. The initial, intrinsic gas-phase conformational diversity of neutral molecules (macrocycle **1** and acids HX), anions X^-, and anionic complexes **1** + X^- was obtained via comprehensive molecular mechanics simulations with the MMFF force field utilizing the Monte Carlo algorithm, implemented in the molecular modeling package Spartan,[31] followed by the semiempirical PM7 calculations using the semiempirical molecular orbital package MOPAC2016.[32] The lowest energy structures within an energy window of 12 kcal·mol^{-1} were next optimized by DFT methods in Gaussian 16.[33] The DFT method comprised an initial optimization using a low-cost Grimme's functional including a dispersion correction B97D and a 6-31G(d′) basis set. The conformational minima were selected based on the B97D energies. Further reoptimization using a tight optimization criterion and thermal analysis (1 atm, 298.15 K) were performed at the PBE1PBE (PBE0)[34] hybrid functional and the 6-311++G**basis set supplemented with the GD3BJ empirical dispersion correction. A quasi-rigid rotor harmonic oscillator approximation was used to account for low-frequency vibration modes ($\nu < 100$ cm^{-1}) and to obtain correct entropy values. The energies of the complexes were additionally corrected by basis set superposition errors. For the selected complexes, the additional dissociation energy calculations were performed using the ωB97XD and Truhlar M06-2X global hybrid functional. The natural bond orbital calculations were performed in Gaussian 16.

The CCSs were calculated by the cavity surface area approximation (Table S1, Supporting Information).[17] The CCS values calculated by this approach well correspond to the CCS obtained from the projection approximation method, taking advantage of the linear relationship between the surface area and the hard sphere collision integral.[35]

The physically meaningful components of the interaction energy between the macrocycle and the anion, that is, electrostatic, exchange, induction, and dispersion terms, were computed by SAPT[30] with the available density-fitting procedure with DF-fitted integrals at the SAPT0/jun-cc-pVTZ level of theory with the PSI4 package.[36] All S2-approximated exchange terms were scaled according to the proposed scaling scheme with the recommended exponent.[37]

ASSOCIATED CONTENT

Ⓢ Supporting Information

The Supporting Information is available free of charge at https://pubs.acs.org/doi/10.1021/acs.joc.0c00917.

> PA and GPB definitions, CCSs, superimposed crystal and theoretical structures, theoretical structures of 1 + X^-, relationships between experimental and theoretical stabilities, PA, and GPB, SAPT0 correlation, xyz coordinates and E$_0$, E$_0$+BSSE, ZPVE, H$_{term}$, and TS of the relevant structures (PDF)

AUTHOR INFORMATION

Corresponding Author

Magdalena Zimnicka − Mass Spectrometry Group, Institute of Organic Chemistry, Polish Academy of Sciences, 01-224 Warszawa, Poland; Ⓞorcid.org/0000-0001-5078-4374; Email: magdalena.zimnicka@icho.edu.pl

Authors

Kinga Kozłowska − Mass Spectrometry Group, Institute of Organic Chemistry, Polish Academy of Sciences, 01-224 Warszawa, Poland

Witold Danikiewicz − Mass Spectrometry Group, Institute of Organic Chemistry, Polish Academy of Sciences, 01-224 Warszawa, Poland; ⓄForcid.org/0000-0003-0484-2689

Complete contact information is available at:

Notes

The authors declare no competing financial interest.

■ REFERENCES

(1) Khan, S.; Ali, J. Chemical analysis of air and water. In *Bioassays*; Häder, D.-P., Erzinger, G. S., Eds.; Elsevier, 2018; Chapter 2, pp 21−39.

(2) Molina, P.; Zapata, F.; Caballero, A. Anion Recognition Strategies Based on Combined Noncovalent Interactions. *Chem. Rev.* **2017**, *117*, 9907−9972.

(3) Liu, Y.; Sengupta, A.; Raghavachari, K.; Flood, A. H. Anion Binding in Solution: Beyond the Electrostatic Regime. *Chem* **2017**, *3*, 411−427.

(4) Hay, B. P.; Firman, T. K; Moyer, B. A. Structural Design Criteria for Anion Hosts: Strategies for Achieving Anion Shape Recognition through the Complementary Placement of Urea Donor Groups. *J. Am. Chem. Soc.* **2005**, *127*, 1810−1819.

(5) Amendola, V.; Boiocchi, M.; Colasson, B.; Fabbrizzi, L. Metal-Controlled Assembly and Selectivity of a Urea-Based Anion Receptor. *Inorg. Chem.* **2006**, *45*, 6138−6147.

(6) Amendola, V.; Bergamaschi, G.; Boiocchi, M.; Fabbrizzi, L.; Milani, M. The Squaramide versus Urea Contest for Anion Recognition. *Chem.—Eur. J.* **2010**, *16*, 4368−4380.

(7) Nehra, A.; Bandaru, S.; Yarramala, D. S.; Rao, C. P. Differential Recognition of Anions with Selectivity towards F− by a Calix[6]-arene-Thiourea Conjugate Investigated by Spectroscopy, Microscopy, and Computational Modeling by DFT. *Chem.—Eur. J.* **2016**, *22*, 8903−8914.

(8) Liu, W.; Oliver, A. G.; Smith, B. D. Stabilization and Extraction of Fluoride Anion Using a Tetralactam Receptor. *J. Org. Chem.* **2019**, *84*, 4050−4057.

(9) Szumna, A.; Jurczak, J. A New Macrocyclic Polylactam-Type Neutral Receptor for Anions − Structural Aspects of Anion Recognition. *Eur. J. Org. Chem.* **2001**, *2001*, 4031−4039.

(10) Meot-Ner Mautner, M. M. *Ion Thermochemistry Data by in NIST Chemistry WebBook*, NIST Standard Reference Database Number 69; Linstrom, P. J., Mallard, W. G., Eds.; National Institute of Standards and Technology: Gaithersburg MD 20899, 2019, (retrieved May 15, 2019).

(11) Thomson, B. A.; Douglas, D. J.; Corr, J. J.; Hager, J. W.; Jolliffe, C. L. Improved Collisionally Activated Dissociation Efficiency and Mass Resolution on a Triple Quadrupole Mass Spectrometer System. *Anal. Chem.* **1995**, *67*, 1696−1704.

(12) Wood, K. V.; Grange, A. H.; Taylor, J. W. Mass Discrimination Effects in a Quadrupole Mass Spectrometer. *Anal. Chem.* **1978**, *50*, 1652−1654.

(13) Drahos, L.; Vékey, K. MassKinetics: a Theoretical Model of Mass Spectra Incorporating Physical Processes, Reaction Kinetics and Mathematical Descriptions. *J. Mass Spectrom.* **2001**, *36*, 237−263.

(14) Chen, Y.-L.; Campbell, J. M.; Collings, B. A.; Konermann, L.; Douglas, D. J. Stability of a Highly Charged Noncovalent Complex in the Gas Phase: Holomyoglobin. *Rapid Commun. Mass Spectrom.* **1998**, *12*, 1003−1010.

(15) Marzluff, E. M.; Campbell, S.; Rodgers, M. T.; Beauchamp, J. L. Collisional Activation of Large Molecules Is an Efficient Process. *J. Am. Chem. Soc.* **1994**, *116*, 6947−6948.

(16) Meroueh, O.; Hase, W. L. Collisional Activation of Small Peptides. *J. Phys. Chem. A* **1999**, *103*, 3981−3990.

(17) Mehmood, A.; Janesko, B. G. Predicting Ion Mobility Collision Cross Sections Directly from Standard Quantum Chemistry Software. *J. Mass Spectrom.* **2018**, *53*, 432−434.

(18) Muir, A. K. S.; Codding, P. W. Structure-activity studies of β-carbolines. 2. Crystal and molecular structures of N-ethyl-3-carbamoyl-β-carboline. *Can. J. Chem.* **1984**, *62*, 1803−1806.

(19) Alcock, N. W.; Moore, P.; Reader, C. J.; Roe, S. M. Synthesis and co-ordination chemistry of two penta-azamacrocycles containing a 1,4-piperazine backbone. Crystal structure determinations of 6,12-dioxo-1,5,13,17,22-penta-azatricyclo[15.2.2.17,11]docosa-7(22),8,10-triene and 1,5,13,17,22-penta-azatricyclo[15.2.2.17,11]docosa-7(22),8,10-trienenickel(II) perchlorate. *J. Chem. Soc., Dalton Trans.* **1988**, 2959−2963.

(20) Hamuro, Y.; Geib, S. J.; Hamilton, A. D. Oligoanthranilamides. Non-Peptide Subunits That Show Formation of Specific Secondary Structure. *J. Am. Chem. Soc.* **1996**, *118*, 7529−7541.

(21) Amendola, V.; Fabbrizzi, L.; Mosca, L. Anion Recognition by Hydrogen Bonding: Urea-Based Receptors. *Chem. Soc. Rev.* **2010**, *39*, 3889−3915.

(22) Parr, R. G.; Pearson, R. G. Absolute Hardness: Companion Parameter to Absolute Electronegativity. *J. Am. Chem. Soc.* **1983**, *105*, 7512−7516.

(23) Pearson, R. G. The Principle of Maximum Hardness. *Acc. Chem. Res.* **1993**, *26*, 250−255.

(24) Chmielewski, M.; Jurczak, J. Size Complementarity in Anion Recognition by Neutral Macrocyclic Tetraamides. *Tetrahedron Lett.* **2004**, *45*, 6007−6010.

(25) Bordwell, F. G. Equilibrium Acidities in Dimethyl Sulfoxide Solution. *Acc. Chem. Res.* **1988**, *21*, 456−463.

(26) Bordwell, F. G.; Algrim, D. Nitrogen acids. 1. Carboxamides and sulfonamides. *J. Org. Chem.* **1976**, *41*, 2507−2508.

(27) Olmstead, W. N.; Bordwell, F. G. Ion-Pair Association Constants in Dimethyl Sulfoxide. *J. Org. Chem.* **1980**, *45*, 3299−3305.

(28) Chai, J.-D.; Head-Gordon, M. Long-range corrected hybrid density functionals with damped atom-atom dispersion corrections. *Phys. Chem. Chem. Phys.* **2008**, *10*, 6615−6620.

(29) Zhao, Y.; Truhlar, D. G. The M06 Suite of Density Functionals for Main Group Thermochemistry, Thermochemical Kinetics, Noncovalent Interactions, Excited States, and Transition Elements: Two New Functionals and Systematic Testing of Four M06-Class Functionals and 12 Other Functionals. *Theor. Chem. Acc.* **2008**, *120*, 215−241.

(30) Jeziorski, B.; Moszynski, R.; Szalewicz, K. Perturbation Theory Approach to Intermolecular Potential Energy Surfaces of van der Waals Complexes. *Chem. Rev.* **1994**, *94*, 1887−1930.

(31) *Spartan'16*. Wavefunction, Inc.: Irvine, CA, 2016.

(32) Stewart, J. J. P. *MOPAC2016*. HTTP://OpenMOPAC.net; Stewart Computational Chemistry: Colorado Springs, CO, USA, 2016.

(33) Frisch, M. J.; Trucks, G. W.; Schlegel, H. B.; Scuseria, G. E.; Robb, M. A.; Cheeseman, J. R.; Scalmani, G.; Barone, V.; Petersson, G. A.; Nakatsuji, H.; Li, X.; Caricato, M.; Marenich, A. V.; Bloino, J.; Janesko, B. G.; Gomperts, R.; Mennucci, B.; Hratchian, H. P.; Ortiz, J. V.; Izmaylov, A. F.; Sonnenberg, J. L.; Williams; Ding, F.; Lipparini, F.; Egidi, F.; Goings, J.; Peng, B.; Petrone, A.; Henderson, T.; Ranasinghe, D.; Zakrzewski, V. G.; Gao, J.; Rega, N.; Zheng, G.; Liang, W.; Hada, M.; Ehara, M.; Toyota, K.; Fukuda, R.; Hasegawa, J.; Ishida, M.; Nakajima, T.; Honda, Y.; Kitao, O.; Nakai, H.; Vreven, T.; Throssell, K.; Montgomery, J. A., Jr.; Peralta, J. E.; Ogliaro, F.; Bearpark, M. J.; Heyd, J. J.; Brothers, E. N.; Kudin, K. N.; Staroverov, V. N.; Keith, T. A.; Kobayashi, R.; Normand, J.; Raghavachari, K.; Rendell, A. P.; Burant, J. C.; Iyengar, S. S.; Tomasi, J.; Cossi, M.; Millam, J. M.; Klene, M.; Adamo, C.; Cammi, R.; Ochterski, J. W.;

Martin, R. L.; Morokuma, K.; Farkas, O.; Foresman, J. B.; Fox, D. J. *Gaussian 16*, Revision B.01: Wallingford, CT, 2016.

(34) Adamo, C.; Barone, V. Toward Reliable Density Functional Methods Without Adjustable Parameters: The PBE0 Model. *J. Chem. Phys.* **1999**, *110*, 6158−6170.

(35) Shvartsburg, A. A.; Jarrold, M. F. An Exact Hard-Spheres Scattering Model for the Mobilities of Polyatomic Ions. *Chem. Phys. Lett.* **1996**, *261*, 86−91.

(36) Turney, J. M.; Simmonett, A. C.; Parrish, R. M.; Hohenstein, E. G.; Evangelista, F. A.; Fermann, J. T.; Mintz, B. J.; Burns, L. A.; Wilke, J. J.; Abrams, M. L.; Russ, N. J.; Leininger, M. L.; Janssen, C. L.; Seidl, E. T.; Allen, W. D.; Schaefer, H. F.; King, R. A.; Valeev, E. F.; Sherrill, C. D.; Crawford, T. D. Psi4: An Open-Source Ab Initio Electronic Structure Program. *Wiley Interdiscip. Rev.: Comput. Mol. Sci.* **2012**, *2*, 556−565.

(37) Parker, T. M.; Burns, L. A.; Parrish, R. M.; Ryno, A. G.; Sherrill, C. D. Levels of Symmetry Adapted Perturbation Theory (SAPT). I. Efficiency and Performance for Interaction Energies. *J. Chem. Phys.* **2014**, *140*, 094106.